FSSP Characterization with Monodisperse Water Droplets

M. WENDISCH AND A. KEIL

Physics Department, Institute for Tropospheric Research, Leipzig, Germany

A. V. KOROLEV

Cloud Physics Research Division, Atmospheric Environment Service, Toronto, Ontario, Canada

(Manuscript received 2 January 1996, in final form 25 April 1996)

ABSTRACT

A droplet generator was used to calibrate and study some features of the forward-scattering spectrometer probe (FSSP). The generator produces a stable jet of monodisperse droplets with the rate of 50–500 droplets per second and a velocity between 0.4 and 1.3 m s^{-1}. The estimated standard deviation of the diameter of the droplets is not larger than 1%. Because of the low rate of generated droplets, there were no coincidence problems during the measurements, that is, no multiple droplets in the laser beam. The results of FSSP calibration in its operating ranges 0 and 1 are presented in this paper. The experiments revealed minor differences (<15%) to the size calibration given by the manufacturer. A comparison of the measurements with theoretical Mie curves yielded good agreement.

Furthermore, the effects of the laser beam inhomogeneity on the droplet sizing were studied. Scanning the droplet jet perpendicular and parallel to the axis of the laser beam of the FSSP showed that underestimates of the droplet size up to 9 μm measured by the FSSP may occur. The undersizing depends on the position, in which the droplets cross the sample volume, and the size of the droplets. This contributes to artificial broadening of the size spectra by the FSSP. An algorithm for droplet spectra retrieval due to light inhomogeneity and particle velocity is discussed.

The results obtained during this study were obtained using one specific FSSP owned by the Institute for Tropospheric Research. However, the range of effects will certainly be similar for other FSSPs.

1. Introduction

The forward-scattering spectrometer probe (FSSP) manufactured by Particle Measuring Systems Inc. (PMS) (Boulder, Colorado) is the most commonly used instrument to measure the droplet size distribution and liquid water content (LWC) of liquid clouds. The principle of operation of the FSSP has been summarized by Knollenberg (1981). Monochromatic laser radiation is scattered in the forward direction by individual particles passing through the laser beam and is collected within the solid angle range between about 3° and 13°. The scattered light is converted into an electric pulse, and the pulse amplitude is sized by a 15-channel pulse height analyzer (PHA).

There has been a number of studies of response characteristics and calibrations of the FSSP. These can be split into two directions. First, one is the theoretical calibration based on the Mie scattering calculations (Pinnick and Auvermann 1979; Pinnick et al. 1981; Cerni 1983; Dye and Baumgardner 1984; Kim and Boatman 1990; Jaenicke and Hanusch 1993). The calculations were done in assumption of plane-parallel uniform wave. The main questions under solution were intercomparisons with PMS calibration, the effect of collecting angle, refractive index, and oscillations of the Mie scattering curve on sizing and broadening of the measured size distribution. Hovenac and Lock (1993) performed calculations of FSSP calibration based on Mie scattering while taking into account the multimode structure of the laser beam.

The second direction of these studies is represented by laboratory calibrations. Because of difficulties in producing stable monodisperse droplets, almost all researches have used glass beads with known size distribution (Gayet 1976; Pinnick and Auvermann 1979; Cerni 1983; Dye and Baumgardner 1984). The difference in scattering between glass beads and water droplets were considered by Mie calculations. It was found that the FSSP undersizes and artificially broadens the size distribution. Different authors tried to explain these effects by particle coincidence in the sample volume (Baumgardner et al. 1985; Cooper 1988), limited response time of the electronics (Cerni 1983; Dye and

Corresponding author address: Dr. Manfred Wendisch, Institute for Tropospheric Research, Permoserstr. 15, 04303 Leipzig, Germany.
E-mail: wendisch@tropos.de

Baumgardner 1984; Korolev et al. 1985a; Baumgardner and Spowart 1990), wrong calibration, or oscillations of Mie scattering curve (Cerni 1983; Dye and Baumgardner 1984; Korolev et al. 1985b). Another likely reason of droplet spectrum broadening is the light intensity inhomogeneity within the sample volume (Baumgardner and Spowart 1990).

This paper presents the results of FSSP characterization by monodisperse droplets in the diameter range of 18–47 μm. The result of laboratory calibrations were compared to manufacturer's one and Mie calculations. The sample volume was scanned by means of a high-stable water droplet jet to study the light inhomogeneity and its influence on droplet sizing on an experimental basis. It was found that the profile of light intensity within the sample volume may lead to considerable undersizing and broadening of droplet size distribution. From the scanning measurements, the retrieval matrices for the droplet spectra reconstruction were calculated. Furthermore, the influence of droplet velocity on FSSP response was studied theoretically.

2. Description of the installation

a. Droplet generator

The droplet generator used in this study is similar to that one described by Korolev et al. (1985b; 1991). The original prototype of this generator was designed by Binek and Dohnalova (1967). Different versions of this generator type were used by Abbot and Cannon (1972), Neizvestny (1972), and Cannon and Grotewold (1980). The generator is based on the principle of tearing off a small droplet by a needle that is quickly withdrawn from a fluid meniscus. A diagram of the droplet generator is shown in Fig. 1. A fiber glass needle with a diameter between 30 and 50 μm is attached to a vibrating spring made from magnetic material. The motion of the spring is driven by an electromagnet, which is controlled by an audio oscillator. To excite the spring's motion, the frequency of the oscillator must be close to the resonance frequency of the spring. In this study we used several resonance frequencies between 50 and 500 Hz. The oscillations of the spring cause the needle to periodically immerse into a liquid (in our case distilled water) meniscus. This is formed in a vertical slit cut in a glass capillary tube, which is supplied by a water reservoir.

The size of generated droplets depends on the following parameters: (a) diameter, shape, and hydrophilic property of the needle; (b) frequency and amplitude of the needle vibration; (c) meniscus shape; (d) angle between needle and meniscus surface at the moment of the needle withdraw from the liquid; (e) velocity of the needle at the moment of its withdrawal from the liquid; and (f) the viscosity and surface tension of the liquid.

Gradual adjustment of the above parameters allowed a smooth change of the droplet size. For example, the meniscus shape was controlled by the width of the slit of the capillary tube and the water pressure. The water pressure in the capillary tube was governed by the elevation of the water level in the water reservoir connected to the capillary tube by flexible hose. For fine adjustment of the meniscus shape the water reservoir was placed on a two-dimensional (2D) positioning stage. The resonance frequency was controlled by the length and mass of the spring. Item (d) was managed by the relative position of the spring with respect to the capillary tube, which was adjusted by means of a three-positioning stage. Item (e) was determined by the amplitude of the needle vibration.

The droplets were generated at the same frequency as the spring's vibration. The falling droplets formed a very narrow and stable jet. Since the distance between generated droplets was much greater than the FSSP la-

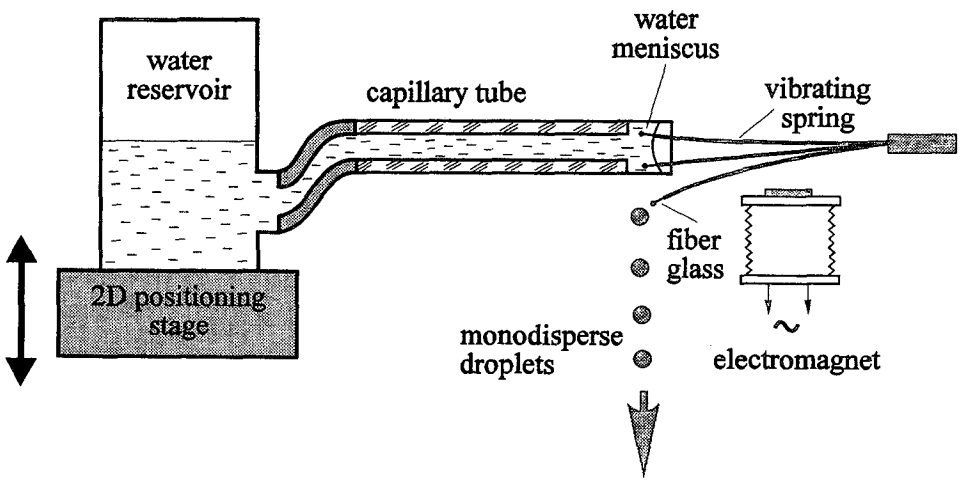

FIG. 1. Sketch of the droplet generator assembly (side view, not scaled).

ser beam diameter, there was no coincidence, that is, multiple particles in the laser beam.

The initial velocity of droplets was of the order of 1 m s^{-1}. Due to air friction droplets decelerate and finally fall with Stokes velocity. The characteristic way of deceleration for droplets having a size between 10 and 50 μm is several millimeters. Over the distance of the laser beam (approximately 0.2 mm) the change of droplet velocity was negligible. The distance between water meniscus and sample volume of FSSP was about 1 mm. This distance is necessary for damping out the droplet oscillations, which arise at the moment of the droplet tearing off from the meniscus.

b. Calibration installation

The whole droplet generator was mounted on a three-dimensional (3D) positioning stage (Fig. 2) that allowed the ejection of the monodisperse droplets into specific locations of the laser beam of the FSSP. The generator assembly was placed between the two FSSP horns. The capillary tube was mounted on another 3D positioning stage for accurate adjustment of the vibrating needle within the vertical slit.

The aspiration tube was removed from the FSSP and optical alignment of the FSSP was performed beforehand. To minimize the influence of external vibration that may disturb the stability of the generator, the FSSP and droplet generator were placed on a massive optical table. Small droplets are very sensitive to any air motion, which leads to destabilization of the droplet jet. Therefore, the droplet generator and the FSSP sample volume were carefully isolated from environment by two nested plastic housings. The FSSP was operated in the "normal mode" (Kim and Boatman 1990), which is recommended by the manufacturer for sampling speeds below 25 m s^{-1}.

The FSSP signal induced by the droplets passing through the sample volume were measured at two different points within the FSSP electronics: (i) in the photodetector module (PMS 410) before the first programmable amplifier (FSSP operating manual) and (ii) in the pulse height analyzer module (PMS 402, pin B/2). These two signals U_{PHOT} and U_{PHA} were recorded by a digital oscilloscope, which also provides accumulation and averaging of the signals. Two examples of the oscilloscope records at the photodetector U_{PHOT}

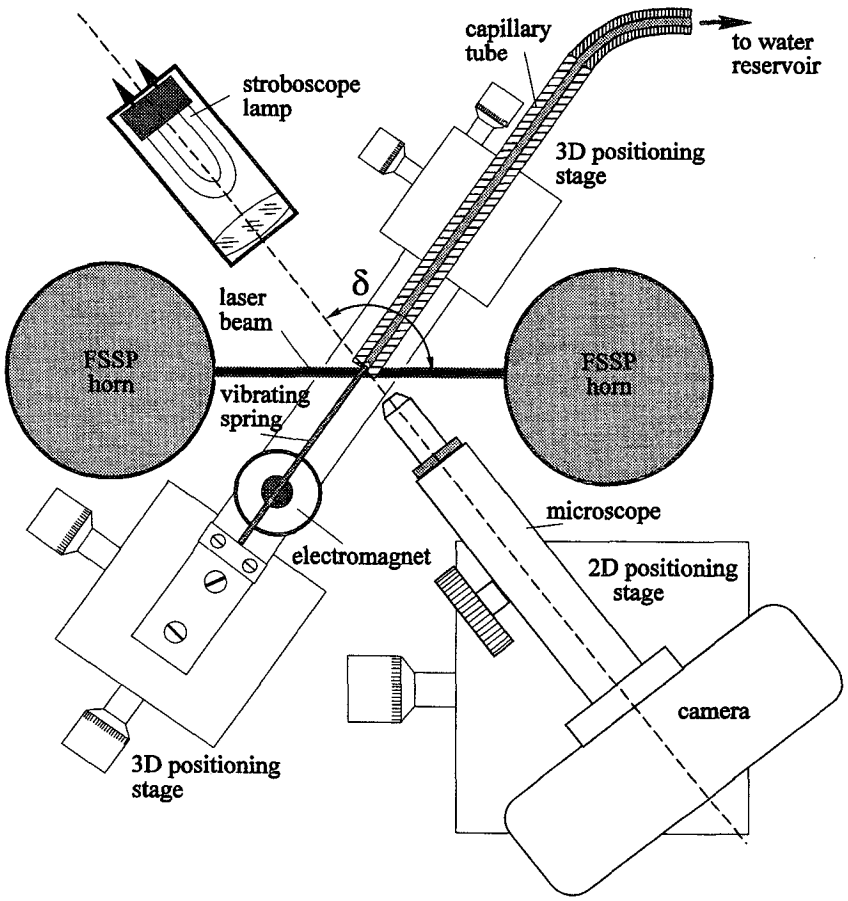

FIG. 2. Sketch of the experimental setup (top view, not scaled).

are presented in Figs. 3 and 4. The lower, strongly fluctuating curve represents a signal for a single droplet. The upper, smooth curve shows the average signal for several thousand droplets of the same size. The curves are offset from one another to show the signal features. A detailed discussion of Figs. 3 and 4 is given in section 4a.

c. *Measurements of droplet sizes*

Droplet sizes were measured in three different ways. The first method entails sizing droplet images directly from microphotographs. Pictures were taken by a camera (Fig. 2) through a microscope in stroboscopic light. The flashing of the strobe lamp was synchronized by the leading edge of the *transit gate signal* from the FSSP (see FSSP operating manual). The manually controlled delay of the triggering of the strobe lamp was used for accurate positioning of the image of the droplet in the microscope viewfield. Usually the delay was adjusted so that the flash of the strobe lamp is triggered when a droplet is in the sample volume of the FSSP.

The second method consisted of measuring the distance between two glares (Korolev et al. 1991), which appear when the droplet passes through the laser beam. One of the glares results from reflected light, and another one from refracted light. The glares arise only if the angle between axis of the microscope and laser beam δ is ranged within $100° < \delta < 180°$. The distance between glares d_{gl} is related to the droplet diameter d_{true} in the following way (see appendix A):

$$\frac{d_{gl}}{d_{true}} = \frac{1}{2}\left\{\frac{n\cos(\delta/2)}{[1 + n^2 - 2n\sin(\delta/2)]^{1/2}} + \sin\left(\frac{\delta}{2}\right)\right\}, \quad (1)$$

where n is the real part of refractive index of water ($n = 1.332$) at the wavelength of the FSSP laser. The range of angles of observation $120° < \delta < 130°$ yields the maximum precision of droplet sizing, since the value d_{gl}/d_{true} is almost independent on δ (see appendix A). This angle range was used in our laboratory installation.

The third method used to size the droplets was based on the measurements of the frequency of oscillations of the droplet shape that arise just after tearing off the water meniscus. Figure 5 demonstrates the variation of the photodetector signal U_{PHOT} at the initial moment of the droplet formation. Periodic variation of the signal was indicated by the variations of scattered light resulting from oscillations of the droplet shape. The frequency of the droplets oscillations was approximately 35 kHz. The amplitude of oscillations damped out due to the liquid viscosity after about 280 μs. After the oscillations disappeared, the droplets diameter was approximately 44 μm. Using Eqs. (10-92) and (10-91) of Pruppacher and Klett (1978), we got a droplet diameter of about 43 μm, which is in good agreement with our photographic measurements.

During our measurements the first two methods for droplet sizing were normally used. These two approaches have the advantages that the pictures of droplet images and glares were directly taken in the sample volume, that is, at the moment of its sizing by the FSSP.

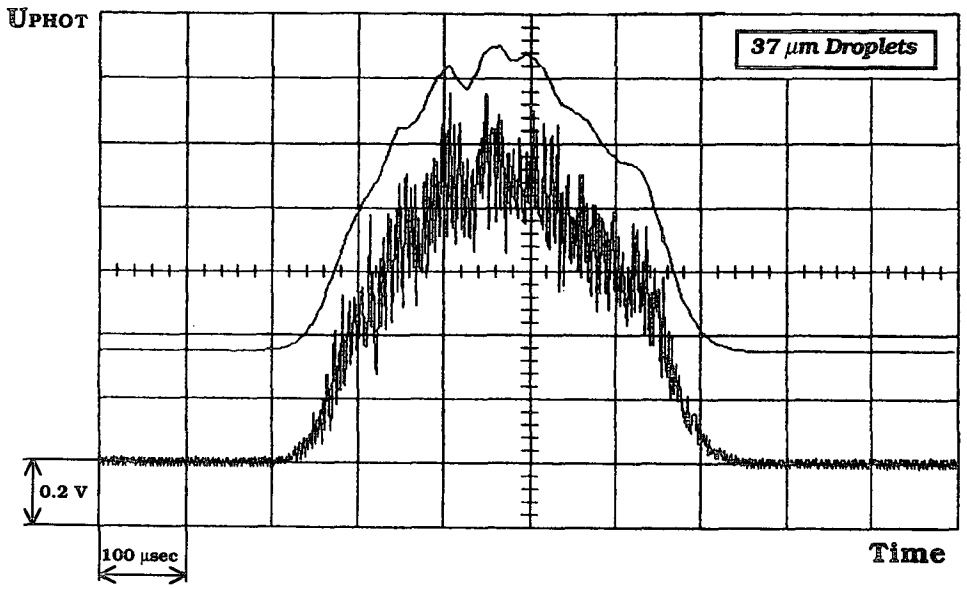

FIG. 3. Oscilloscope screen plot of the photodetector signal U_{PHOT} for 37-μm droplets. The vertical division is 0.2 V; the horizontal division is 100 μs. The upper curve represents an average signal for several thousand droplets; the lower curve shows the signal for a single droplet.

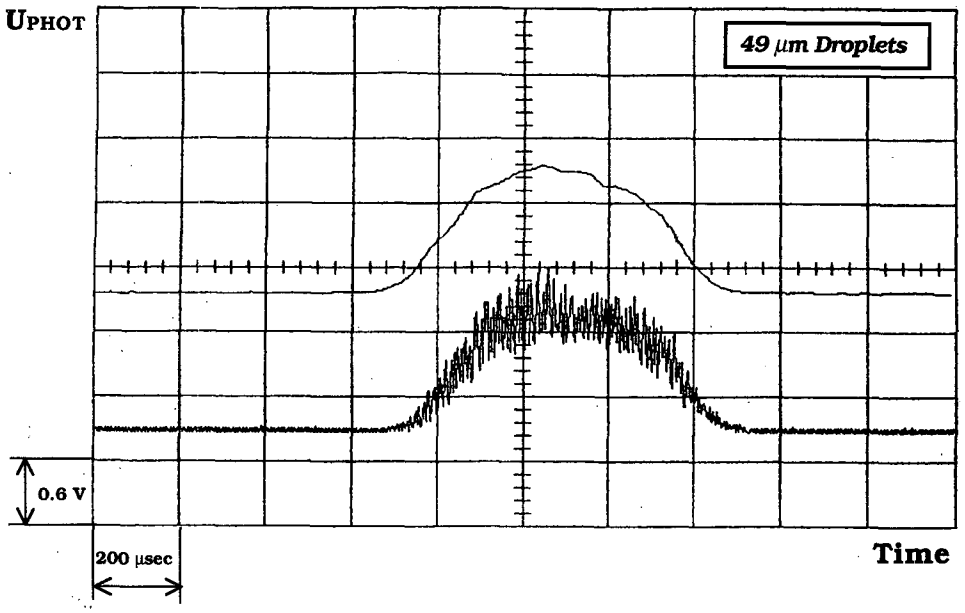

FIG. 4. Oscilloscope screen plot of the photodetector signal U_{PHOT} for 49-μm droplets. The vertical division is 0.6 V; the horizontal division is 200 μs. The upper curve represents an average signal for several thousand droplets; the lower curve shows the signal for a single droplet.

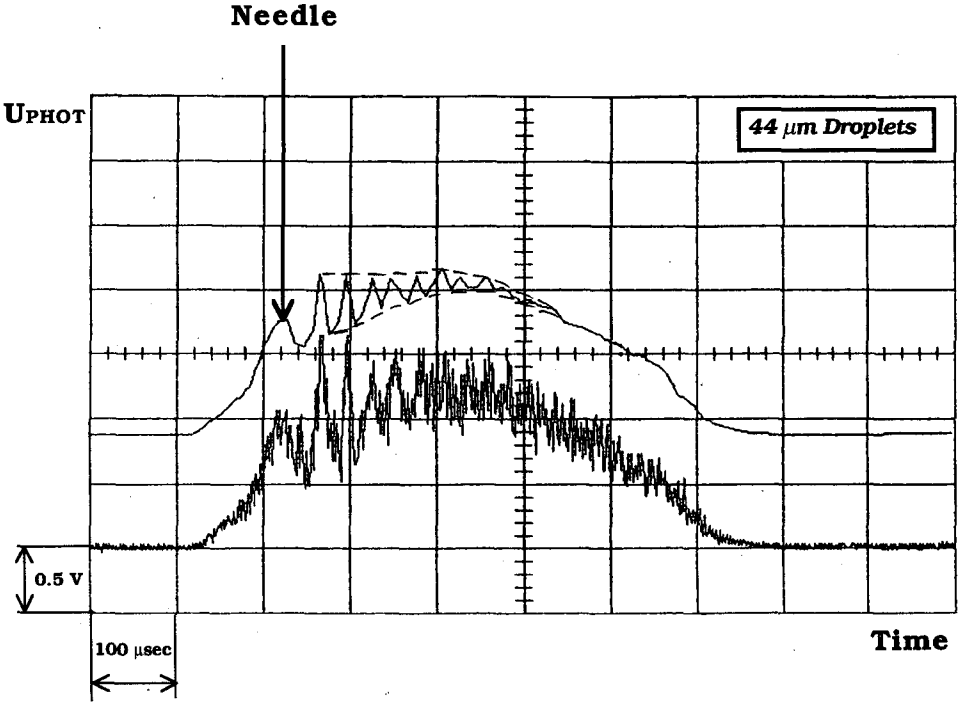

FIG. 5. Oscilloscope screen plot of the photodetector signal U_{PHOT} for oscillating droplets shortly after their formation. The vertical division is 0.5 V, and the horizontal division is 100 μs. The upper curve represents an average signal for several thousand droplets; the lower curve shows the signal for a single droplet. The dashed lines indicate the attenuation of the droplet oscillations. The first peak corresponds to the scattering signal of the needle.

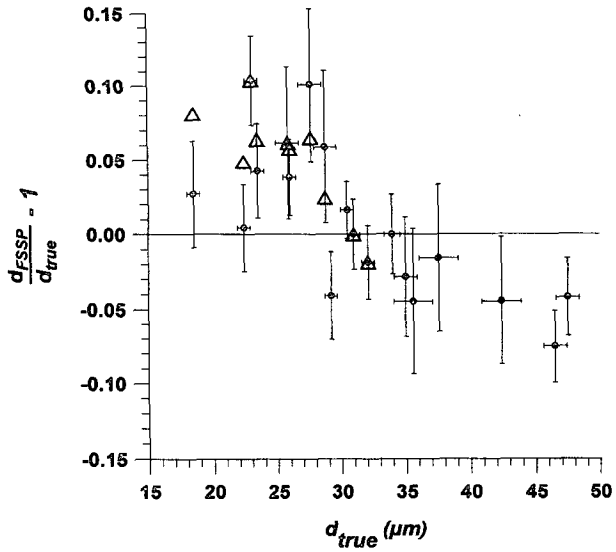

FIG. 6. Calibration results for operating ranges 0 and 1 of the FSSP. Nineteen droplet sizes between 18- and 47-μm diameter were used for calibration of range 0 (dots). The open triangles represent the results for range 1 with 10 droplet sizes between 18- and 32-μm diameter.

The second method (glare distance measurement) provided more accurate results of droplet sizes since the glares give more sharp images on the microphotographs compared to the flashed droplets.

Analysis of numerous pictures taken during calibrations showed high stability of the generated droplets. The standard deviation of droplet diameter was estimated to be not larger than 1%.

3. Calibrations

a. Calibration by monodisperse droplets

The calibrations of the FSSP in its operating ranges 0 and 1 were fulfilled for droplets in the size range from 18 to 47 μm. The monodisperse droplets were generally counted by the FSSP in only one channel. Droplets were registered in two channels only if its size were close to the channel threshold. Thus, the FSSP size distributions were much narrower than the ones from glass beads.

The peak voltage of the FSSP signal at the input of PHA was calculated as

$$\langle U_{\mathrm{PHA}} \rangle = |U_{\mathrm{PHA}}| + \frac{1}{2} U_{\mathrm{noise}}. \qquad (2)$$

Here $|U_{\mathrm{PHA}}|$ is the peak voltage of the *averaged* signal at the input of PHA module, and U_{noise} is the width of the noise from a *single* particle record near the maximum of the average signal. The peak voltage $\langle U_{\mathrm{PHA}} \rangle$ was normalized by the reference voltage of the laser intensity, and then the FSSP droplet size d_{FSSP} was approximated by stepwise linear interpolation of the PHA threshold voltages given by the manufacturer.

Figure 6 shows the results of the calibration for the FSSP operating ranges 0 and 1. The difference between d_{FSSP} and d_{true} is plotted in a normalized way in dependence of the true droplet diameter d_{true}. The horizontal error bars represent 20% of U_{noise} transformed into droplet diameters. The vertical bars result from the errors of the droplet sizing by microphotographs and of d_{true}. To avoid confusion in the figure, the error bars for the calibration results in range 1 (triangles) were omitted. They have the same order of magnitude as the error bars for the measurements in range 0. All droplet sizes were determined by the method of glare distance measurement, except the three droplet sizes with d_{true} = 35.6, 37.6, and 42.4 μm, which were determined directly from the flashed droplet images.

Figure 6 indicates a good agreement between the FSSP and actual droplet size between 30 and 40 μm for both FSSP operating ranges. The droplets with smaller diameters were mostly oversized by the FSSP, while the larger ones were undersized. This behavior was also reported by Dye and Baumgardner (1984). However, the deviation from manufacturer's size calibration did not exceed 15% (about 2 μm), which is in the order of the size resolution of the FSSP in range 1. The best-fit calibrating curves are as follows:

$$d_{\mathrm{true}} = 1.2 d_{\mathrm{FSSP}} - 5.1 \qquad (3a)$$

for the FSSP operating range 0 and

$$d_{\mathrm{true}} = 1.1 d_{\mathrm{FSSP}} - 5.0 \qquad (3b)$$

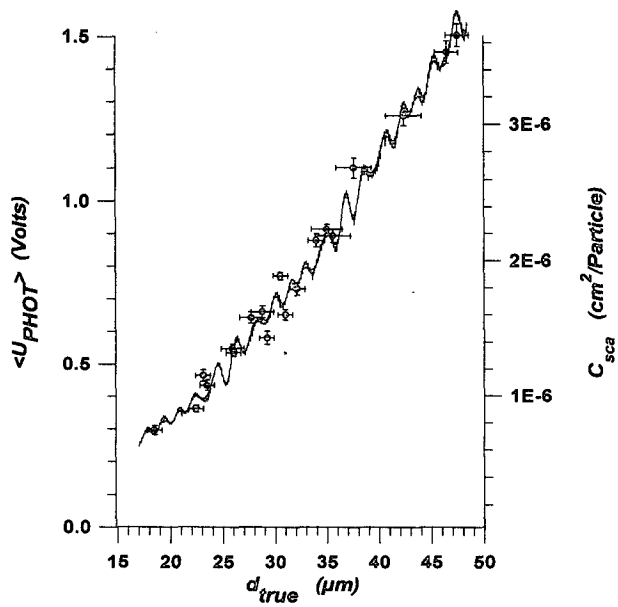

FIG. 7. Comparison between measured peak voltages $\langle U_{\mathrm{PHOT}} \rangle$ (dots, left scale) and calculated scattering response C_{sca} (solid curve, right scale) in dependence of true droplet diameter d_{true}. The droplet diameter ranged from 18 to 47 μm. Nineteen droplet sizes are included.

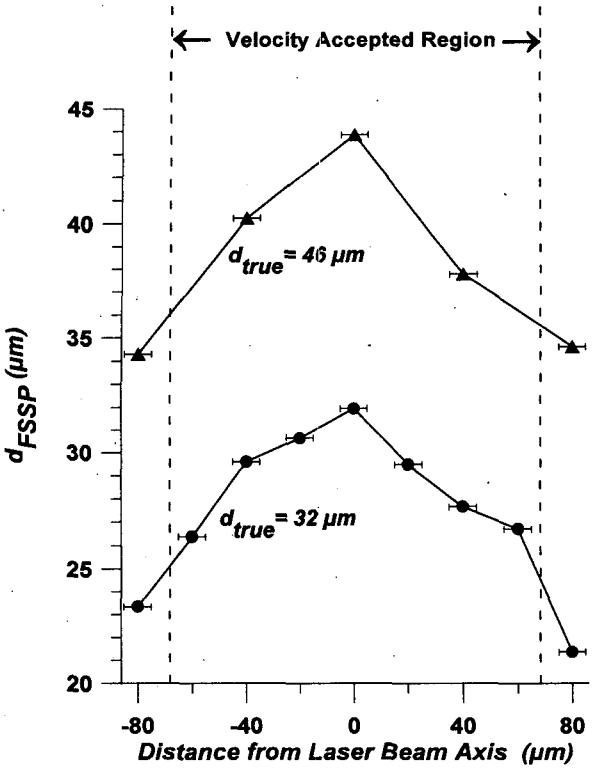

FIG. 8. Scanning measurements perpendicular to the laser beam axis in the center of depth of field in range 0 of the FSSP. The droplet sizes are d_{true} = 46 μm (triangles) and d_{true} = 32 μm (dots). The diameter d_{FSSP} obtained from the peak voltage $\langle U_{PHA}\rangle$ is plotted in dependence of the distance from the laser beam axis. The dashed lines represent the boundaries of the theoretical velocity accepted region (VAR = 0.62).

for the FSSP operating range 1. Here d_{true} and d_{FSSP} are in microns. The coefficients of correlation are 0.98 and 0.97 for FSSP operating ranges 0 and 1, respectively.

The experiments were performed with slow-moving droplets (0.4–1.3 m s^{-1}). The FSSP electronics is designed for much higher droplet velocities. However, measurements with an electronic pulse generator simulating droplets with low velocity show that the slow moving droplets are not undersized as a result of the FSSP electronics.

b. Comparison with Mie calculations

The results of the calibration were compared with Mie scattering calculations. In assumption of plane-parallel uniform waves, the radiation scattered by a spherical particle in the axis symmetric collecting angle is represented by the scattering cross section C_{sca} (Bohren and Huffmann 1983):

$$C_{sca}(n_w, d_{true}, \lambda) = \frac{\lambda^2}{4\pi}\int_{\psi_1}^{\psi_2} [j_1(n_w, d_{true}, \lambda, \psi') + j_2(n_w, d_{true}, \lambda, \psi')] \sin\psi' d\psi'. \quad (4)$$

Here n_w is the complex refractive index of the particle. In our case we had water droplets with $n_w = 1.332 - 1.39 \times 10^{-8}\, i$, d_{true} is the droplet diameter; λ is the wavelength, in our case the wavelength of the FSSP laser, (λ = 0.6328 μm); ψ is the scattering angle ($\psi_1 = 3.1°$ and $\psi_2 = 13.0°$); j_1 and j_2 are intensity distribution functions that were calculated on the basis of Mie theory after Deirmendjian (1969) with the recursion formula by Lentz (1976).

Figure 7 shows the comparison of Mie calculations and laboratory measurements. The calibrating curve was built as a dependence of droplet size on peak amplitude of the FSSP photodetector signal $\langle U_{PHOT}\rangle$, which was determined in the same manner as $\langle U_{PHA}\rangle$ from the oscilloscope record [cf. Eq. (2)]. The calibration and Mie curves were scaled to minimize the squared difference between $\langle U_{PHOT}\rangle$ and C_{sca}. This yielded the following scaling equation:

$$\langle U_{PHOT}\rangle = FC_{sca} - 0.015$$

with

$$F = 0.415\text{E+}06 \text{ V cm}^{-2}.$$

Generally, the calibrating curve was in good agreement with the Mie calculations. Some differences may be caused by uncertainties in droplet sizing or measurements of signal peak amplitude during calibrations.

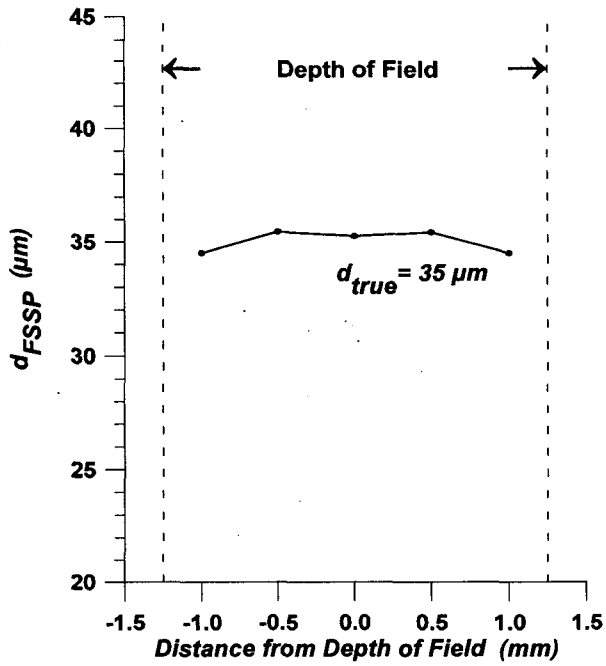

FIG. 9. Scanning measurements along the laser beam axis in the center of the laser beam cross section in range 0 of the FSSP. The size of the droplets was d_{true} = 35 μm. The diameter d_{FSSP} obtained from the peak voltage $\langle U_{PHA}\rangle$ is plotted in dependence of the distance from the center of depth of field. The boundaries of depth of field are marked by the dashed lines.

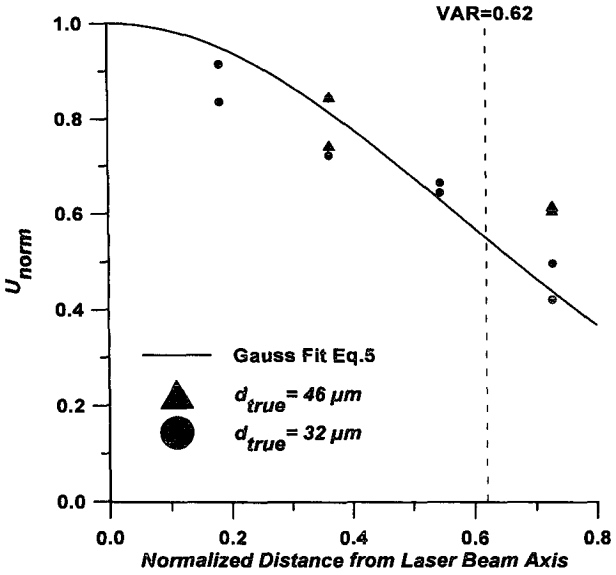

FIG. 10. Normalized averaged light intensity distribution along the laser beam cross section [Eq. (5)]. The measurements from Fig. 8 are added (dots for 32-μm droplets and triangles for 46-μm droplets).

4. Inhomogeneity of light intensity of the sample volume

a. Crosswise inhomogeneity

Figures 3 and 4 demonstrate the light inhomogeneity across the laser beam. It shows that the signal from 37-μm droplets (Fig. 3) had fluctuations in the central part of the laser beam. These fluctuations were caused by multimodal structure of the laser used in FSSP (Baumgardner and Spowart 1990; Hovenac and Lock 1993). The signal from 49-μm droplets (Fig. 4) was much smoother than that of 37-μm droplets. This was due to the fact that the diameter of the 49-μm droplet was larger than the characteristic distance between laser modes. The fluctuations of the intensity scattered by a single droplet passing through the laser beam turned out to be less than that predicted by Hovenac and Lock (1993). This may be caused by differences in lasers or by small fluctuations of the droplet jet. The latter may lead to smoothing of the averaged signal.

To reduce the influence of light inhomogeneity on particle sizing, droplets passing close to the edges of laser beam are rejected by the FSSP electronics. The rejection is based on comparisons of the particle transit time with the current average transit time of the droplets. If the transit time is longer than the average transit time, the particle is velocity accepted. Otherwise it is velocity rejected. The particle is counted only if it crosses the laser beam within the depth of field and the velocity accepted region. The depth of field limits the sample volume along the axis of the laser beam, while the velocity accepted region limits the sample volume in the direction perpendicular to the axis of the laser beam. The theoretical value of velocity accepted ratio (VAR), that is, the ratio of velocity accepted region to the laser beam diameter, is 0.62 (Dye and Baumgardner 1984).

To study the effect of the light inhomogeneity on the FSSP response the laser beam was scanned by monodisperse droplet jets in crosswise direction. Figure 8 presents the results of such scanning for 32- and 46-μm droplets. It is seen that within the theoretical velocity accepted region the error in droplet sizing may reach several microns (up to 9 μm). The error of undersizing increased while moving away from the center of the laser axis.

b. Lengthwise inhomogeneity

There have been a number of studies of the inhomogeneity of light intensity in longitudinal direction of FSSP sample volume (Gayet 1976; Dye and Baumgardner 1984; Korolev et al. 1985a; Cooper 1988), but until now there were no direct measurements of droplet sizing along laser beam axis. Figure 9 shows the results of scanning of the sample volume along the laser beam axis by a droplet jet consisting of 35-μm droplets. The scanning was conducted

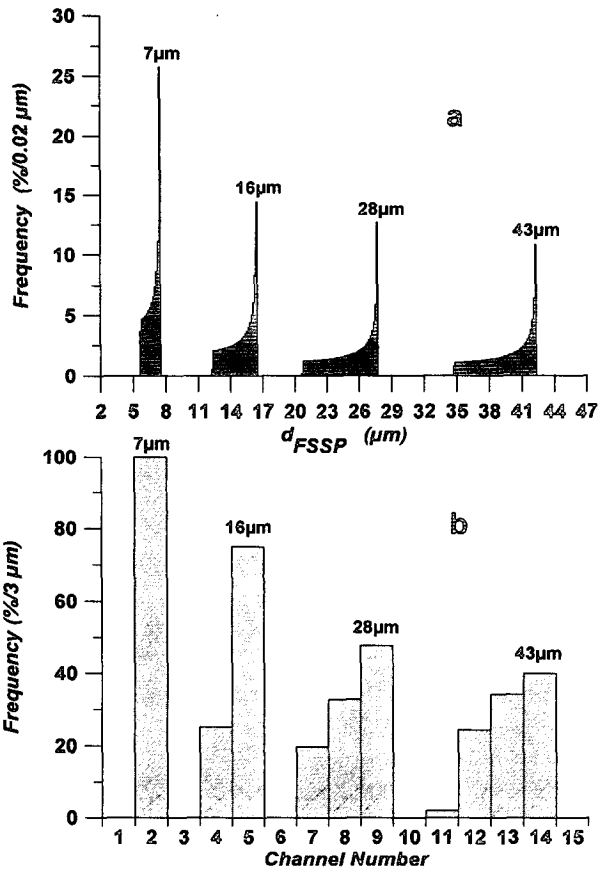

FIG. 11. (a) Calculated frequency distribution for the different droplet sizes 7, 16, 28, and 43 μm with a size resolution of 0.02 μm. The PMS calibration curve was fitted by a quadratic polynomial. (b) Same as (a) with a size resolution of 3 μm.

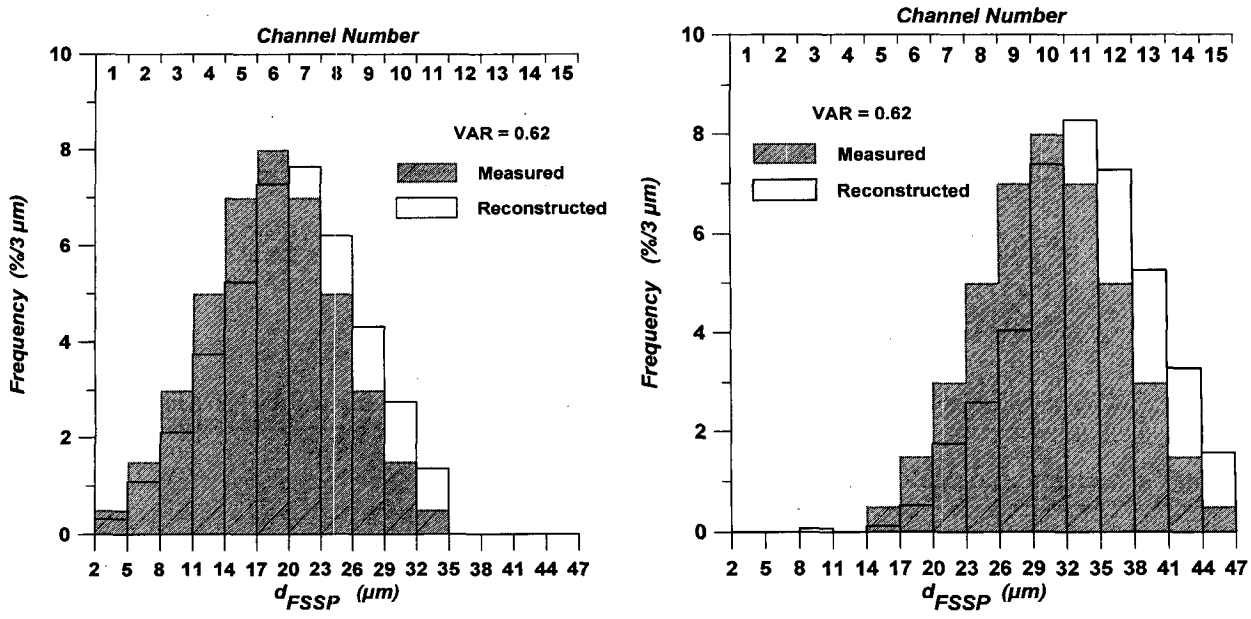

FIG. 12. (a) Comparison between measured (given) and reconstructed (actual) size spectra for a size distribution with mode diameter of 18.5 μm. (b) Same as in (a) for a size distribution with mode diameter of 30.5 μm.

within the depth of field. As it is seen, the influence of light inhomogeneity on the particle sizing was much smaller along the laser axis (in the range of 1 μm). The droplets were counted generally in one FSSP channel.

5. Droplet spectra distortion and retrieval procedure

The PHA peak voltage $\langle U_{\text{PHA}} \rangle$ for the two droplet sizes 32 and 46 μm collected during the crosswise scanning measurements (see also Fig. 8) were normalized to the respective peak voltage measured in the center of the laser beam cross section. Then these normalized data were fitted in terms of a Gaussian distribution. The resulting Gaussian curve (Fig. 10) was accepted as an average light intensity distribution in the crosswise direction of the laser beam and used in the following calculations. It has the form

$$U_{\text{norm}} = \exp\left[-\left(\frac{y}{0.8}\right)^2\right]. \tag{5}$$

Here y is the normalized distance from the laser beam axis, $y = 1$ represents the radius of the laser beam cross section (110 μm), and $y = 0$ is the center of the laser beam. For comparison the measurements from Fig. 8 are added in Fig. 10.

A numerical algorithm was used in order to describe the FSSP response. The droplets were assumed to pass randomly within the sample volume, which was limited by the depth of field and the velocity accepted region. On the basis of Eq. (5) and the FSSP calibration curve, distorted size distributions were calculated for different monodisperse spectra (Fig. 11a). The same calculations were performed for the discrete FSSP channel thresholds (Fig. 11b). It is seen that the droplet spectra broadening to smaller diameters occurs due to partly undersizing of droplets. The amount of undersized droplets clearly increases with increasing droplet size. For droplets of 40–45-μm diameter, the effect of spectrum broadening reaches up to four FSSP channels. However, for the droplets within the size range of the first four FSSP channels in range 0 (2–14 μm), the spectrum broadening is negligible.

From the calculation of the response spectrum for droplets, uniformly distributed in each channel, we get the distortion matrix $\mathbf{R}$, such that

$$\mathbf{s}_m = \mathbf{R}\mathbf{s}_a. \tag{6}$$

Here $\mathbf{s}_m$ is the 15×1 matrix of the measured FSSP droplet spectrum, $\mathbf{s}_a$ represents the 15×1 matrix of the actual droplet size distribution, and $\mathbf{R}$ is the 15×15 distortion matrix describing the measurement characteristics of the FSSP. The coefficients of the matrix $\mathbf{R}$ for the FSSP operating range 0 are given in appendix B.

Using the inverted matrix $\mathbf{R}^{-1}$, we obtain the actual droplet size distribution as

$$\mathbf{s}_a = \mathbf{R}^{-1}\mathbf{s}_m. \tag{7}$$

Figures 12a and 12b give examples of the reconstructed [by inversion of Eq. (6)] actual size spectrum on the basis of a given measurement for two different size distributions measured by the FSSP in operating range 0. The distortion is roughly equivalent to shifting the whole spectrum one channel down. As expected, the undersizing effect is more pronounced for the spectrum

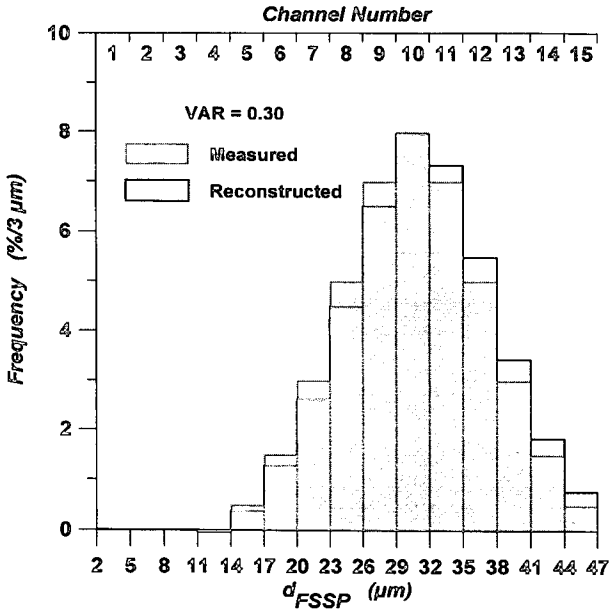

FIG. 13. The same as in Fig. 12b for a velocity accepted ratio of 0.3.

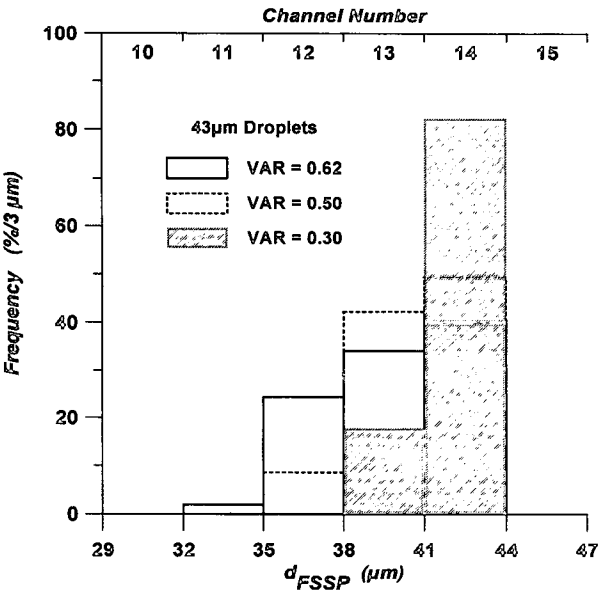

FIG. 14. Calculation of the broadening effect for monodisperse droplets of 43-μm diameter for the different velocity acceptance ratios 0.62, 0.5, and 0.3.

with larger mode diameter (Fig. 12b). For both cases the LWC calculated on the basis of FSSP measured spectrum is 23% less than that obtained from the reconstructed (actual) spectrum, while the calculated effective radius is 7% less than actual one.

The above retrievals were done for the case when the velocity accepted ratio is 0.62. The same calculations were fulfilled for assumed velocity accepted ratios of 0.5 and 0.3. In these cases the distortion is much less than for the first case and measured and reconstructed (actual) spectra are almost coincide. This is because the smaller VAR limits the laser beam inhomogeneity. For an assumed VAR of 0.3 (Fig. 13), the underestimation of LWC and effective radius are 6% and 2%, respectively.

Figure 14 demonstrates the decrease of droplet spectra distortion while VAR decreases from 0.62 to 0.3 for monodisperse droplets of 43-μm diameter. The decrease of velocity accepted region is equivalent to the reduction of the light inhomogeneity in the sample volume. For the VAR of 0.3, the measured size spectrum is almost monodisperse.

The matrix $\mathbb{R}$ (appendix B) was calculated only for small droplet velocities. If the droplet velocity exceeds 50–60 m s^{-1}, the response time of the electronics is necessary to take into account (Cerni 1983; Korolev et al. 1985a; Baumgardner and Spowart 1990). This will lead to a change of the matrix $\mathbb{R}$.

To evaluate this effect, the matrix $\mathbb{R}$ was calculated for 25 and 100 m s^{-1} droplet velocity on the basis of the signal amplitude dependency on particle velocity in the PHA module, measured by Korolev et al. (1985a) using a spinning sic with a fiber glass. The normalized FSSP signal for the velocity range from 60 to 150 m s^{-1} was described as

$$f = a + bv, \tag{8}$$

where v represents the droplet velocity (m s^{-1}). The coefficients a and b depend on the operating range of the FSSP. For range 0 we have a = 1.05 and b

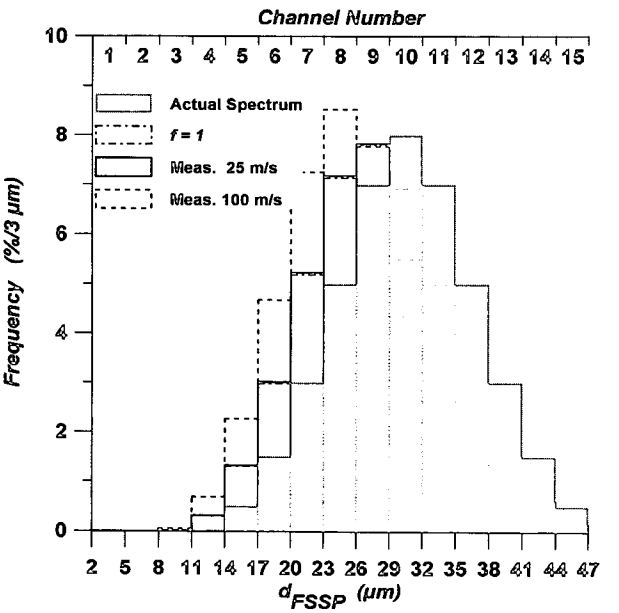

FIG. 15. Comparison between actual droplet size spectrum s_a (given) and measured spectrum s_m for the different droplet velocities v = 25 m s^{-1} and v = 100 m s^{-1}. VAR = 0.62, FSSP operating range 0.

$= -2.17e\text{-}3$. The calculated matrices **R** for the droplet velocities 25 and 100 m s^{-1} are given in appendix C. To estimate the influence of droplet velocity on the measured size spectrum, the matrices **R** for the different droplet velocities were used in Eq. (6) together with a given actual spectrum s_a. The resulting measured (by the FSSP) droplet spectra $\mathbf{s}_m$ are shown in Fig. 15. The curve for $f = 1$ represents the effect of laser beam inhomogeneity only. The difference between measured and actual droplet spectrum increases with velocity. For 25 m s^{-1} (ground-based operation of FSSP) this difference is mainly caused by laser beam inhomogeneity and not by droplet velocity. For 100 m s^{-1} the measurement of the FSSP underestimates the actual droplet size roughly by two channels. The LWC calculated on the basis of FSSP measured spectrum is 41% less than the actual one, while the calculated effective radius is 16% less than the real one for the droplet velocity of 100 m s^{-1}.

6. Conclusions

The droplet generator presented in this paper has been proven to be a reliable tool to study some characteristics of the FSSP in detail. The generator produces monodisperse droplets with an estimated standard deviation not larger than 1%. Scanning the sample volume by monodisperse droplets showed the variation of scattered light caused by the multimode structure of the FSSP laser. The oscillations were found to be less than predicted by Hovenac and Lock (1993). The calibration of our FSSP showed minor differences to the PMS size calibration not exceeding 15% (about 2 μm). A comparison with theoretical Mie curves yielded good agreement. A scanning of the laser beam in the crosswise direction by the droplet jet has shown that the undersizing of droplets may reach up to 9 μm near the edges of 0.62 velocity accepted region for droplets of 40–47 μm. Scanning the laser beam in the direction parallel to the laser beam axis within depth of field yields an uncertainty of about 1 μm. Numerical calculations have shown that a droplet spectrum distortion caused by the light intensity inhomogeneity in the crosswise direction to the laser beam may lead to underestimation of LWC of about 23% and of effective radius of about 7%.

All the experimental results given in this paper were obtained using the FSSP (S/N 31303-0693-149) owned by the Institute for Tropospheric Research. However, the general conclusions drawn from the measurements can be extended to other FSSPs because the principle problems of FSSP are inherent in the measurement principle and do not depend on the special instrument used.

Acknowledgments. This paper contains parts of the master thesis of one of the authors (A. Keil). Jost Heintzenberg supported this work by stimulating discussions and valuable comments. Dave Covert is acknowledged for helpful suggestions to the manuscript.

APPENDIX A

Formation of Droplet Glares

Figure A1 shows the formation of glares caused by a droplet that is illuminated by a collimated laser

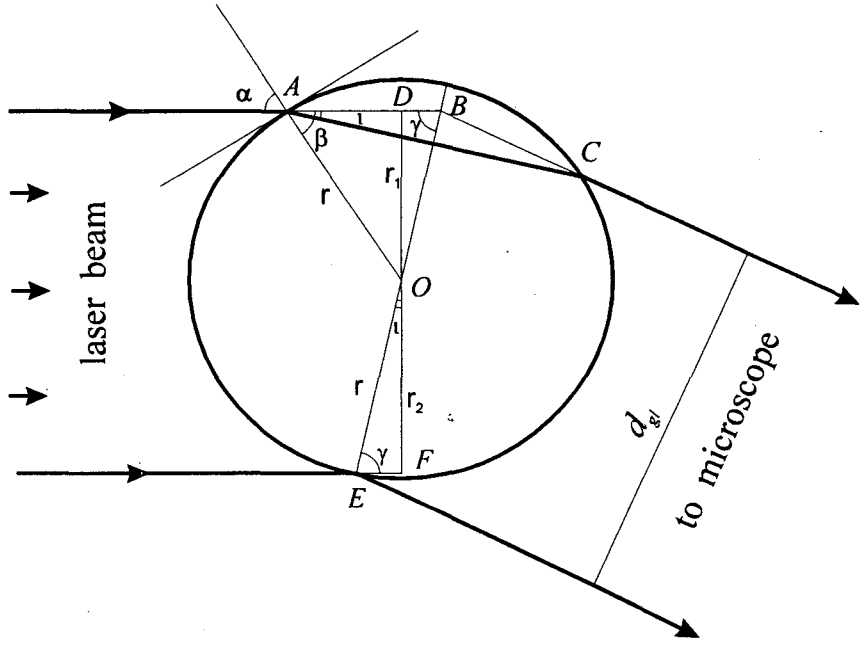

FIG. A1. Geometry for glare distance calculation.

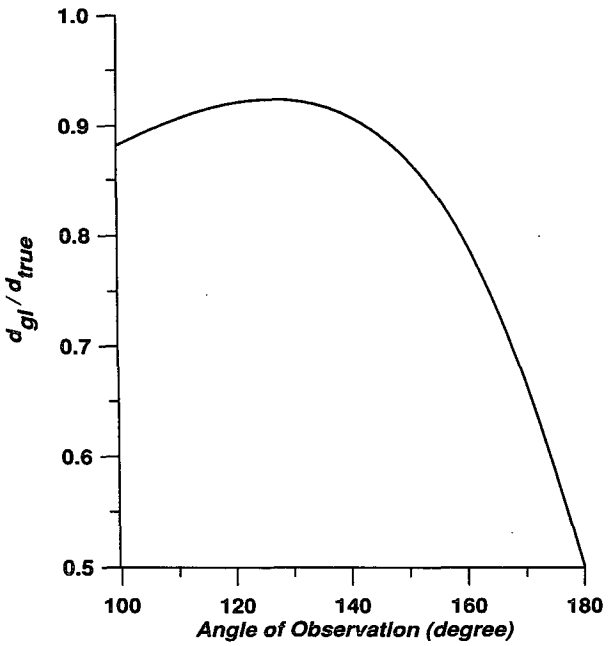

FIG. A2. Ratio of glare distance d_{gl} and droplet diameter d_{true} in dependence of the angle of observation δ.

light beam. The lower glare results from reflected light, and the upper one from refracted light. The droplet is assumed to move perpendicular through the laser beam.

Let us find the ratio d_{gl}/d_{true}, with $d_{true} = 2r$ the droplet diameter, and d_{gl} the distance between glares. The distance between glares d_{gl} can be written as

$$d_{gl} = r_1 + r_2. \tag{A1}$$

From the triangle *ADO* follows

$$r_1 = r \sin\alpha. \tag{A2}$$

Substituting Snellius equation $\sin\alpha/\sin\beta = n$ into Eq. (A2), we get

$$\sin\beta = \frac{r_1}{nr}. \tag{A3}$$

Here α is the incident angle, β is an angle of refraction, and n is the real part of refractive index of water. The relation between angles α, β, and γ can be written as

$$\alpha = \beta + \iota = \beta + \frac{\pi}{2} - \gamma.$$

Using this equality, we find

$$\sin\alpha = \cos\beta \cos\gamma + \sin\beta \sin\gamma. \tag{A4}$$

Here γ is one-half of the angle of observation $\angle ABC = \delta = 2\gamma$.

Substituting (A2) and (A3) into (A4) and excluding α and β, we obtain

$$\frac{r_1}{r} = \frac{n \cos\gamma}{(1 + n^2 - 2n \sin\gamma)^{1/2}}. \tag{A5}$$

From the triangle *OEF* we get

$$r_2 = r \sin\gamma. \tag{A6}$$

Thus, combining (A1), (A5), and (A6), we finally obtain

$$\frac{d_{gl}}{d_{true}} = \frac{1}{2}\left[\frac{n \cos\gamma}{(1 + n^2 - 2n \sin\gamma)^{1/2}} + \sin\gamma\right]. \tag{A7}$$

Figure A2 shows the dependence of the ratio d_{gl}/d_{true} on the angle of observation $\delta = 2\gamma$. The range of angles of observation $120° < \delta < 130°$ yields the maximum precision of droplet sizing, since there the value d_{gl}/d_{true} is almost independent on δ.

APPENDIX B

Distortion Matrix R for FSSP Operating Range 0 for Low Droplet Velocity

1.0000	0.1740	0.0000	0.0000	0.0000	0.0000	0.0000	0.0000	0.0000	0.0000	0.0000	0.0000	0.0000	0.0000	0.0000
0.0000	0.8260	0.2871	0.0000	0.0000	0.0000	0.0000	0.0000	0.0000	0.0000	0.0000	0.0000	0.0000	0.0000	0.0000
0.0000	0.0000	0.7129	0.3839	0.0131	0.0000	0.0000	0.0000	0.0000	0.0000	0.0000	0.0000	0.0000	0.0000	0.0000
0.0000	0.0000	0.0000	0.6161	0.4366	0.0575	0.0000	0.0000	0.0000	0.0000	0.0000	0.0000	0.0000	0.0000	0.0000
0.0000	0.0000	0.0000	0.0000	0.5503	0.4406	0.1202	0.0000	0.0000	0.0000	0.0000	0.0000	0.0000	0.0000	0.0000
0.0000	0.0000	0.0000	0.0000	0.0000	0.5019	0.4154	0.1822	0.0100	0.0000	0.0000	0.0000	0.0000	0.0000	0.0000
0.0000	0.0000	0.0000	0.0000	0.0000	0.0000	0.4644	0.3836	0.2225	0.0396	0.0000	0.0000	0.0000	0.0000	0.0000
0.0000	0.0000	0.0000	0.0000	0.0000	0.0000	0.0000	0.4342	0.3583	0.2350	0.0830	0.0000	0.0000	0.0000	0.0000
0.0000	0.0000	0.0000	0.0000	0.0000	0.0000	0.0000	0.0000	0.4092	0.3373	0.2273	0.1264	0.0092	0.0000	0.0000
0.0000	0.0000	0.0000	0.0000	0.0000	0.0000	0.0000	0.0000	0.0000	0.3881	0.3197	0.2149	0.1549	0.0325	0.0000
0.0000	0.0000	0.0000	0.0000	0.0000	0.0000	0.0000	0.0000	0.0000	0.0000	0.3700	0.3045	0.2043	0.1649	0.0662
0.0000	0.0000	0.0000	0.0000	0.0000	0.0000	0.0000	0.0000	0.0000	0.0000	0.0000	0.3542	0.2913	0.1951	0.1607
0.0000	0.0000	0.0000	0.0000	0.0000	0.0000	0.0000	0.0000	0.0000	0.0000	0.0000	0.0000	0.3402	0.2797	0.1870
0.0000	0.0000	0.0000	0.0000	0.0000	0.0000	0.0000	0.0000	0.0000	0.0000	0.0000	0.0000	0.0000	0.3278	0.2694
0.0000	0.0000	0.0000	0.0000	0.0000	0.0000	0.0000	0.0000	0.0000	0.0000	0.0000	0.0000	0.0000	0.0000	0.3166

APPENDIX C

Distortion Matrix R for FSSP Operating Range 0 for Droplet Velocity v = 25 and 100 m s^{-1}

v = 25 m s^{-1}

1.0000	0.1774	0.0000	0.0000	0.0000	0.0000	0.0000	0.0000	0.0000	0.0000	0.0000	0.0000	0.0000	0.0000	0.0000
0.0000	0.8226	0.2929	0.0000	0.0000	0.0000	0.0000	0.0000	0.0000	0.0000	0.0000	0.0000	0.0000	0.0000	0.0000
0.0000	0.0000	0.7071	0.3907	0.0141	0.0000	0.0000	0.0000	0.0000	0.0000	0.0000	0.0000	0.0000	0.0000	0.0000
0.0000	0.0000	0.0000	0.6093	0.4433	0.0600	0.0000	0.0000	0.0000	0.0000	0.0000	0.0000	0.0000	0.0000	0.0000
0.0000	0.0000	0.0000	0.0000	0.5426	0.4466	0.1243	0.0000	0.0000	0.0000	0.0000	0.0000	0.0000	0.0000	0.0000
0.0000	0.0000	0.0000	0.0000	0.0000	0.4933	0.4206	0.1865	0.0113	0.0000	0.0000	0.0000	0.0000	0.0000	0.0000
0.0000	0.0000	0.0000	0.0000	0.0000	0.0000	0.4551	0.3893	0.2259	0.0422	0.0000	0.0000	0.0000	0.0000	0.0000
0.0000	0.0000	0.0000	0.0000	0.0000	0.0000	0.0000	0.4242	0.3643	0.2373	0.0869	0.0001	0.0000	0.0000	0.0000
0.0000	0.0000	0.0000	0.0000	0.0000	0.0000	0.0000	0.0000	0.3985	0.3437	0.2286	0.1304	0.0107	0.0000	0.0000
0.0000	0.0000	0.0000	0.0000	0.0000	0.0000	0.0000	0.0000	0.0000	0.3768	0.3264	0.2162	0.1578	0.0353	0.0000
0.0000	0.0000	0.0000	0.0000	0.0000	0.0000	0.0000	0.0000	0.0000	0.0000	0.3580	0.3117	0.2058	0.1666	0.0700
0.0000	0.0000	0.0000	0.0000	0.0000	0.0000	0.0000	0.0000	0.0000	0.0000	0.0000	0.3415	0.2989	0.1966	0.1616
0.0000	0.0000	0.0000	0.0000	0.0000	0.0000	0.0000	0.0000	0.0000	0.0000	0.0000	0.0000	0.3269	0.2877	0.1885
0.0000	0.0000	0.0000	0.0000	0.0000	0.0000	0.0000	0.0000	0.0000	0.0000	0.0000	0.0000	0.0000	0.3139	0.2779
0.0000	0.0000	0.0000	0.0000	0.0000	0.0000	0.0000	0.0000	0.0000	0.0000	0.0000	0.0000	0.0000	0.0000	0.3020

v = 100 m s^{-1}

1.0000	0.3544	0.0000	0.0000	0.0000	0.0000	0.0000	0.0000	0.0000	0.0000	0.0000	0.0000	0.0000	0.0000	0.0000
0.0000	0.6456	0.5575	0.0160	0.0000	0.0000	0.0000	0.0000	0.0000	0.0000	0.0000	0.0000	0.0000	0.0000	0.0000
0.0000	0.0000	0.4425	0.6749	0.1007	0.0000	0.0000	0.0000	0.0000	0.0000	0.0000	0.0000	0.0000	0.0000	0.0000
0.0000	0.0000	0.0000	0.3092	0.6836	0.2184	0.0063	0.0000	0.0000	0.0000	0.0000	0.0000	0.0000	0.0000	0.0000
0.0000	0.0000	0.0000	0.0000	0.2157	0.6353	0.3111	0.0547	0.0000	0.0000	0.0000	0.0000	0.0000	0.0000	0.0000
0.0000	0.0000	0.0000	0.0000	0.0000	0.1463	0.5892	0.3451	0.1333	0.0029	0.0000	0.0000	0.0000	0.0000	0.0000
0.0000	0.0000	0.0000	0.0000	0.0000	0.0000	0.0934	0.5471	0.3379	0.2028	0.0348	0.0000	0.0000	0.0000	0.0000
0.0000	0.0000	0.0000	0.0000	0.0000	0.0000	0.0000	0.0532	0.5040	0.3298	0.2334	0.0930	0.0013	0.0000	0.0000
0.0000	0.0000	0.0000	0.0000	0.0000	0.0000	0.0000	0.0000	0.0248	0.4588	0.3274	0.2305	0.1489	0.0240	0.0000
0.0000	0.0000	0.0000	0.0000	0.0000	0.0000	0.0000	0.0000	0.0000	0.0058	0.4043	0.3325	0.2229	0.1771	0.0693
0.0000	0.0000	0.0000	0.0000	0.0000	0.0000	0.0000	0.0000	0.0000	0.0000	0.0000	0.3440	0.3452	0.2172	0.1776
0.0000	0.0000	0.0000	0.0000	0.0000	0.0000	0.0000	0.0000	0.0000	0.0000	0.0000	0.0000	0.2816	0.3546	0.2130
0.0000	0.0000	0.0000	0.0000	0.0000	0.0000	0.0000	0.0000	0.0000	0.0000	0.0000	0.0000	0.2271	0.3608	
0.0000	0.0000	0.0000	0.0000	0.0000	0.0000	0.0000	0.0000	0.0000	0.0000	0.0000	0.0000	0.0000	0.1793	
0.0000	0.0000	0.0000	0.0000	0.0000	0.0000	0.0000	0.0000	0.0000	0.0000	0.0000	0.0000	0.0000	0.0000	

REFERENCES

Abbot, C. E., and T. W. Cannon, 1972: A droplet generator with electronic control of size, production rate and charge. *Rev. Sci. Instrum.*, **43,** 1313–1317.

Baumgardner, D., and M. Spowart, 1990: Evaluation of the Forward Scattering Spectrometer Probe. Part III: Time response and laser inhomogeneity limitations. *J. Atmos. Oceanic Technol.*, **7,** 666–672.

——, W. Strapp, and J. Dye, 1985: Evaluation of the Forward Scattering Spectrometer Probe. Part II: Corrections for coincidence and dead-time losses. *J. Atmos. Oceanic Technol.*, **2,** 626–632.

Binek, B., and B. Dohnalova, 1967: Ein Generator zur Herstellung monodisperser Aerosole aus der flüssigen Phase. *Staub-Reinhalt. Luft,* **27,** 492–494.

Bohren, C. F., and D. R. Huffman, 1983: *Absorption and Scattering of Light by Small Particles.* John Wiley & Sons, 530 pp.

Cannon, T. W., and W. W. Grotewold, 1980: Improved drop generators for calibration of drop spectrometers and use in laboratory cloud physics experiments. *J. Appl. Meteor.*, **19,** 901–905.

Cerni, T. A., 1983: Determination of the size and concentration of cloud drops with an FSSP. *J. Climate Appl. Meteor.*, **22,** 1346–1355.

Cooper, W. A., 1988: Effects of coincidence on measurements with a Forward Scattering Spectrometer Probe. *J. Atmos. Oceanic Technol.*, **5,** 823–832.

Deirmendjian, D., 1969: *Electromagnetic Scattering on Spherical Polydispersions.* Elsevier, 292 pp.

Dye, J. E., and D. Baumgardner, 1984: Evaluation of the Forward Scattering Spectrometer Probe. Part I: Electronic and optical studies. *J. Atmos. Oceanic Technol.*, **1,** 329–344.

Gayet, J. F., 1976: Sur les performances de L'ASSP-100 de Knollenberg pour la granulometrie des nuages. *J. Rech. Atmos.*, **10,** 105–118.

Hovenac, E. A., and J. A. Lock, 1993: Calibration of the forward-scattering spectrometer probe: Modeling scattering from a multimode laser beam. *J. Atmos. Oceanic Technol.*, **10,** 518–525.

Jaenicke, R., and T. Hanusch, 1993: Simulation of the optical particle counter Forward Scattering Spectrometer Probe 100 (FSSP-100). Consequences for size distribution measurements. *Aerosol Sci. Technol.*, **18,** 309–322.

Kim, Y. J., and J. F. Boatman, 1990: Size calibration corrections for the Forward Scattering Spectrometer Probe (FSSP) for measurement of atmospheric aerosols of different refractive indices. *J. Atmos. Oceanic Technol.*, **7,** 681–688.

Knollenberg, R. G., 1981: Techniques for probing cloud microstructure. *Clouds, Their Formation, Optical Properties and Effects,* P. V. Hobbs, Ed., A. Deepak, 15–91.

Korolev, A. V., Y. E. Makarov, and V. S. Novikov, 1985a: On the accuracy of photoelectric cloud droplet spectrometer FSSP-100. *Trudi CAO,* **158,** 32–42.

——, ——, and ——, 1985b: On the calibrations of photoelectric cloud droplet spectrometer FSSP-100. *Trudi CAO,* **158,** 43–49.

——, S. V. Kuznetsov, Y. E. Makarov, and V. S. Novikov, 1991: Evaluation of measurements of particle size and sample area from optical array probes. *J. Atmos. Oceanic Technol.,* **8,** 514–522.

Lentz, W. J., 1976: Generating Bessel functions in Mie scattering calculations using continued fractions. *Appl. Opt.,* **15,** 668–671.

Neizvestny, A. I., 1972: Experimental installation for study of collision and coalescence on charged droplets. *Trudi IEM,* **1**(33), 65–74.

Pinnick, R. G., and H. J. Auvermann, 1979: Response characteristics of Knollenberg light-scattering aerosol counters. *J. Aerosol Sci.,* **10,** 55–74.

——, D. M. Garvey, and L. D. Duncan, 1981: Calibration of Knollenberg FSSP light-scattering counters for measurement of cloud droplets. *J. Appl. Meteor.,* **20,** 1049–1057.

Pruppacher, H. R., and J. D. Klett, 1978: *Microphysics of Clouds and Precipitation.* Reidel Publishing, 714 pp.